Effect of Flow Structure on Air-Water Mixing Process at Different Bend Angles

Akeel A. Nazzal and Abdulsattar J. Hasan
Mechanical Engineering Department, University of Technology, Iraq
Email: akeelakeel1992@gmail.com, Abdulsattar.J.Alsarraf@uotechnology.edu.iq

***Abstract*—The secondary flow generated within curved ducts accompanies a substantial change in flow structure due to the imbalance between centrifugal forces and transverse pressure gradient. The current study investigates the effect of changing bend angle on the evaporative cooling of an airstream via spray of water in fogging mode. The experimental Particle image velocimetry (PIV) technique has been implemented for visualizing the secondary flow layout when an air-water mixture travels through the bend duct. The bend angles considered are (45º, 90º and 135º) at velocities of (5, 3.75 and 2.5 m/s) for air flow through 50 cm square duct. PIV results manifested that a single pair of counter rotating vortices appears at 45º bend angle, while the other two bend angles evinced two pairs of vortices (four-cell pattern) across the duct cross-section. The water spray was set to tilt at three orientations, namely (45º, 0º and – 45º) to the axial flow direction to suit the change in bend angle. ANSYS FLUENT 19.R1is used in numerical simulation with RNG-k-ε turbulent model to study the spray characteristics which impacts the cooling process. The best cooling of the airstream is obtained when the water is sprayed axially, i.e. at 0º, prior to the 135º bent duct ranking 30% reduction in temperature corresponding to 6.5% improvement in heat transfer between the two phases.**

***Index Terms*—Curved duct, Secondary flow, Evaporative cooling, Inlet Fogging, (PIVLAB) Technique, Bend angle**

I. Introduction

Flow through bends with different geometries takes an extending role in many engineering applications, like heat exchangers, air-conditioning equipment, aircrafts' intakes, axial compressors inlets, combustors, and many countless areas. The power output and fuel consumption are strongly influenced by the mass flow, quality and the temperature of the ambient air induced into the compressor of the land based gas turbine generators. It is observed that in hot, arid climates during the summer times while the electricity demand peaks, the power output declines due to the less density flow of the inlet air which causes a considerable degradation in the gas turbine performance. Recently the giant manufacturers of power plants like GE, Siemens, ALSTOM, implemented the so-called fogging system to mitigate this deterioration in power production by bringing down the inlet air temperature. Fogging is an effective low cost evaporative cooling which requires least modification to the existing facility. The technique is based on spraying micro-droplets of water into the hot air flow which represents the source of the heat required to vaporise the droplets.

Drastic mixing is essential to produce the higher rates of heat and mass transfer between the suspended droplets and the carrier gas in purpose to enhance the intended air cooling. Gas turbine units comprise inlet ducts with varying configuration those ordinarily include a curved portion prior to the compressor inlet. The most interesting merit with curved channels is the development of the secondary flow vortices which certainly affect mixing due to the intense agitation that helps the droplets to penetrate the surrounding airflow. As the pressure loss along the curved portion is ineluctable, it is advantageous to exploit the naturally developed turbulences within the curved duct to enhance the mixing without exerting additional pressure losses like if intentional turbulence generators are installed behind the spray spot.

The secondary flow is a pair of converse-rotating vortices resulting from the interaction between the viscosity forces and the centrifugal forces. Dean [1] theoretically studied the stability of flow through a curved channel and showed that Dean number is the crucial parameter that rules the structure of the secondary flow within these conduits. An experimental investigation has been conducted on steady, turbulent flow through circular 90º smooth wall bend by Sudu et al [2] at a Reynolds number of 6×10^4 with an aspect ratio of 4. The velocity profiles for the primary and secondary flows were demonstrated, as well as, the Reynolds number distribution across the bend. The results included the discussion of the flow transition in the longitudinal direction. Three-dimensional simulation of the secondary flow for Newtonian and viscoelastic fluids travelling through a square curved duct was performed by Boutabaa et al [3]. Viscoelastic effects were represented by the Phan-Thien-Tanner PTT model. The numerical study adopted three values of Dean numbers 125, 137 and 150 and showed that the two-cells are converted upstream into four-cells pattern with the increase in the centrifugal forces. A can type combustion chamber designed using ANSYS FLUENT code in swirling and non-swirling flows at the inlet under isothermal condition by Al-

Manuscript received May 27, 2022; revised October 1, 2022.

© 2022 Int. J. Mech. Eng. Rob. Res

doi: 10.18178/ijmerr.11.12.923-936

Khafaji and Abdur Rahim [4]. The simulation used the k-ε turbulent model relies on finite volume technique. The results of simulation were validated by comparing them with the experimental data. Arvanitis et al [5] explored numerically the characteristics of heat transfer and flow structure in U-shape curved pipes under partial and full curvature conditions. The computational fluid dynamics software "Open FOAM" was used to perform 3-dimensional steady state simulation on the effect of curvature on heat transfer for the two geometries. Reynolds number has been changed at 100, 1000 and 2000 and the results showed that for moderate and high Re, multiple secondary vortices were detected in fully curved duct. On the other hand, the partially curved duct possessed a more complex flow structure as its effect are stronger for Re =100 and 2000. Nevertheless, fully curved duct surpasses the partially curved at Re= 1000. Laminar, fully developed steam flow has been analysed using ANSYS FLUENT software for bend pipes with different angles focusing on the velocity and pressure distributions. The results of Mondol et al [6] indicted that the velocity and pressure drop for $\theta < 90^0$ are greater than $\theta = 90^o$ and $\theta > 90^o$ bends. The inlet pressure for $\theta < 90^0$ was the highest among the three cases and hence it is recommended to be used in fluid transportation piping systems. Turbulent flow through pipe elbow at different angle was simulated by the k-ε model to characterize the impact of angle and Reynolds number on the single-phase flow separation. Shabani et al [7] determined the pressure loss coefficient for angles between 45^o to 135^o at diverse radius ratio with and without guide vanes. The use of one guide vane appeared beneficial to reduce the loss by 50% for radius ratio of 1.5 for all angles. However, using two guide vanes would bring a higher reduction in loss coefficient. This coefficient seemed to be decreased with increasing Reynolds number.

Fully developed two-dimensional viscous incompressible flow in a curved rectangular duct was investigated numerically relaying on the flow controlling parameter by several researchers. Mondal et al. [8] employed the spectral method to solve the Navier-Stokes equations while using the Crank-Nicolson method to solve the energy equation. Dean Number was considered in the range $1000 \leq Dn \leq 10000$ and Grashof Number within $100 \leq Gr \leq 2000$ in a case where the outer duct wall is kept hot and the inner wall is kept cold while the other walls are considered adiabatic. For $Dn \leq 6400$ it was revealed that the unsteady flow turned steady with increasing Gr. Rotating the curved duct about the curvature centre either positively with unsteady solution for Taylor number $0 \leq Tr \leq 500$, or negatively for $-700 \leq Tr \leq -50$ was performed by Zohurul Islam et al. [9] for the values of Dean number of 1000 and 1500. Changing the aspect ratio of the rectangular duct reflected on the centrifugal-Coriolis and buoyancy forces. The heat generation and thermal enhancement were investigated numerically by Zohurul Islam et al.[10] with a range of Taylor number of $0 \leq Tr \leq 3195$ at aspect ratios of 2 and 3. The heat transfer enhancement is stronger with chaotic flow than with the steady-state or periodic modes due to the act of the secondary flow developed vortices. Hasan et al.[11] explore the Dean vortices development under constant pressure gradient and examine their impact on the heat transfer and transitional flow through a twisted square duct. The study has conducted over the range $-2500 \leq Tr \leq 2500$ while keeping Gr=100, Dn=1000 and curvature ratio of 0.02. The axial flow was shifted to the inner wall in the positive rotation, while shifted outward towards the outer wall in the negative rotation. Time-dependent solution evidenced several flow instabilities including steady-state, periodic, multi-periodic, and chaotic oscillation.

Visualization of the flow field has been approved as a powerful mean to analyse the velocity and structure of flows with variable geometries. Azzola et al [12] employed the Laser-Doppler technique to measure the velocity components of a developing turbulent flow through 180^o curved pipe. A slight change in the longitudinal component was observed beyond $\theta = 90^o$, while the circumferential component did not reach the fully developed state. Reversal of the secondary flow took place independently of the Reynolds number as depicted by the circumferential velocity profile. Semi-elliptic truncation of Reynolds equations was used to predict the flow development along with the k-ε model to surmise the turbulent stress field. Similar findings were obtained by Lee et al [13] whose reported the reach of the secondary flow strength about 28% of the bulk mean velocity when using the hot-wire measurements. Up to the angle 67.5^o, the robust counter-rotating vortex pair are growing up, but beyond $\theta=90^o$, the vortex break down into two-cell pattern. The mean longitudinal velocity component changes little after $\theta=90^o$ in the curved pipe. Jain [14] implemented the refractive index matched, two-dimensional, two-component Particle Image Velocimetry to study the unsteadiness in a turbulent flow through 90^o bent pipe at Re = 34800 and ratio of radius of curvature to the pipe diameter of 1.5 . The study conducted at different planes upstream and downstream the bend. Also the measurements were taken within the bend at angles of 10^o, 20^o, 70^o, 80^o from the inlet. It was clearly observed the formation of the shear layer between the faster fluid close to the outer wall and the slower fluid close to the inner wall along the second half of the bend. The signs of unsteadiness were evident in the secondary flow at 20^o and beyond as two vortices wobbled about the symmetry axis.

Bhattacharya et al [15] submitted a new uncertainty valuation method for the PIV correlated to the probability density function (PDF) of displacements to calculate the moment of correlation (MC). The MC uses the correlation to evaluate the uncertainty in PIV from the correlation plane shape. Gaussian least squares fit is applied to the peak regions representing a discretization of the PDF to account for the peak rotation and stretching caused by the velocity gradients. A better response the

MC method showed to the spatial variation in RMS error and a good agreement was proofed between the predicted uncertainty and the standard uncertainty. Eiamsa-ard et al [16] conducted a visualised heat transfer of a swirling impinging jet created by a nozzle with central helical tape using the thermochromic liquid crystal (TLC). The study covered a ratio of jet-to-plate L/D=2,4,6 and 8 and at Reynolds numbers of range 10000 ≤ Re≤ 20000 to explore their effects on the radial uniformity and convective heat transfer. Experimentally obtained results of the ordinary impinging jets were compared with those obtained by this study. The new results revealed the enhancement of the local and average Nusselt number as the latter is increased with the decrease of the L/D ratio while Re increased for both jets. A 5.3% higher Nu of the swirling impinging jet than that for the ordinary impinging jet was recorded.

Experimental and numerical investigation on the impact of changing the curvature ratio on the flow topology and turbulent intensity in a water-air mixing prior to a curved square duct was performed by Mohammed and Abed-Alfathel [17]. PIV technique was used to visualise the secondary flow structure for curvature ratios 0.25, 0.5 and 0.75 at Re numbers 8×10^4 to 16×10^4. The captured images illustrated the appearance of four-cell pattern for all curvature ratios. The vortex pair close to the inner wall drifted outward with the decrease in curvature ratio due to the centrifugal effect and flow separation. The configuration of the water nozzles array is established in accordance to the numerical simulation using ANSYS FLUENT 19.R1 relying on the RNG k-ε turbulent model. Local temperature and relative humidity mappings were presented along with 3-dimensional velocity and pressure distribution. The study revealed the weak dependence of the mixing on the turbulent intensity while changing Re, however the turbulent intensity was more influenced by the curvature ratio.

The preceding literatures reviewed above indicate the numerous studies recently carried out on the secondary flow development through different geometries curves and bends both experimentally and numerically. However, the most of these studies focus on single-phase fluid flows and some are dealt with moderately high values of Reynolds number in secondary flow analysis, whether for single-phase or Two-phasic flow through curved ducts. Hence, practically there still much opportunities to cover the gap in researches coupling between the secondary flow analysis at different bend geometries and the phase mixing in humidification process at higher Reynolds numbers. In that context, the current study shows how the Dean vortices are produced and transformed from two to four cell patterns at higher Reynolds numbers beyond those adopted previously and evaluate their contribution to the spray cooling with changing bend angle. The present investigation implements the experimental PIV measurements to visualize the flow topology within the curved duct for three bend angles and depicts the liquid droplets dispersion in air flow which affects the rates of heat and mass transfer. Also, the study performs a three dimensional simulation of steady, turbulent incompressible flow through a square duct comprises a curved section using ANSYS FLUENT 19.R1with RNG k-ε turbulent model. The simulation aims predicting the distribution of temperature and relative humidity in purpose indicating their disparity both axially and transversely along the computation domain. The validation of the numerical results is verified using mesh independence test and the obtained results are compared with current acquired experimental data, as well as, with other studies in the respective field. The outcomes of the current study provide the inception point to improve efficiently the performance of many engineering facilities comprising liquid sprays prior to a curved duct. The special investment of this knowledge is in redesign the inlet ducts for gas turbine generators those utilizing fogging systems for power boost by air cooling.

II. Experimental Methods

A. Experimental Set-Up

A 50 cm square duct was employed in this study with details shown in Fig. 1. For the purpose of eliminating the inlet turbulences and ensuring the steadily flowing airstream, a bell mouth shaped duct is installed at the entrance of the test rig. The first 3 m straight duct after the bell mouth is needed to accommodate the preheaters and steam humidifier aiming to fix the inlet air conditions at 45ºC and 15% relative humidity during all the tests.

The mist generator is installed prior to the curved duct with capability to adjust its axial position before the curve. The mist generator comprises an array of nine atomizers which are equally spaced across the duct cross-section. The atomizers are supplied with distillated water provided by the pumping machine working at a pressure of 70 bar. The atomizer has a diameter of 0.1 mm and it has the ability to tilt in a range between 90º to – 90º to axial flow, modifying the entrainment characteristics of the injected droplets within the airflow field. Fig. 2 shows the layout and the applicable limits for the experimental-related adjustable features of the test rig.

The curved duct employed in the study is designed with three different bend angles, namely 45º, 90º and 135º, as evinced in Fig. 3. This design postulates that the change in flow structure would promote mixing between the suspended droplets and the carrier airstream via the secondary flow provoked within the curved duct.

© 2022 Int. J. Mech. Eng. Rob. Res

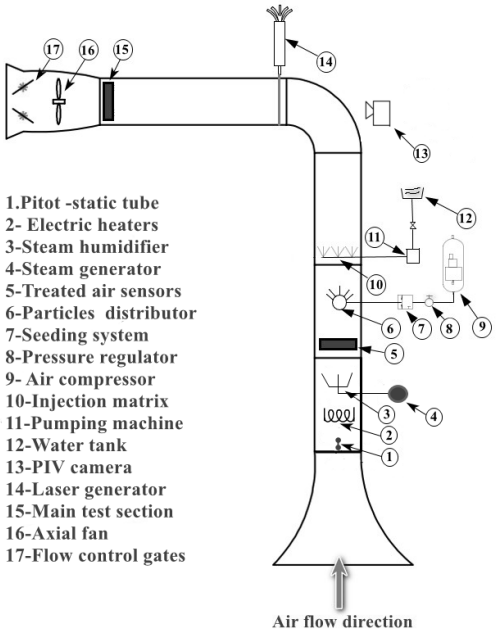

Figure 1. Layout of the test rig

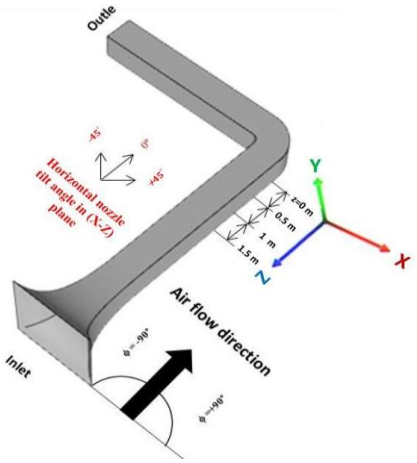

Figure 2. Adjustable limits of the testing parameters

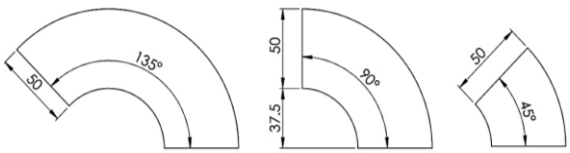

Figure 3. Geometry of curved ducts with different bend angles

The exit of the curved duct is connected to the second 2 m straight duct leading to the axial induction fan which exhausts the treated air out of the duct. The air flow rate is controlled by the butterfly gates fixed at the fan outlet. The air average velocity was measured by a standard elliptical nosed Pitot-static tube installed at the entrance to the first straight duct. ARDOUINO data acquisition system consists of 25 probes evenly distributed over the duct cross section and it is fixed at the main test section located at the fan entrance. The probes collect the moist air temperature and relative humidity and send them to a computer in order to be saved and subsequently analyzed. Four more probes are located after the preheating station, assuring the desired inlet air temperature and relative humidity.

B. Particle Image Velocimetry in MATLAB (PIVLab)

The topology of the secondary flow generated at each bend angle is visualized at the middle plane of the curved duct to study its effect on the mixing of water and airstream. The particle image velocimetry in MATLAB (PIVlab) represents an analytical mean of the PIV that complies with the particles seeding system. The metallic titanium dioxide TiO_2 particles are used and illuminated by a laser sheet, while a high-speed camera being used to capture the flow field images, see Fig. 4. Compressed air

© 2022 Int. J. Mech. Eng. Rob. Res

under pressure of 3 bar is needed to eject particles out of the seeder and introduce them into airstream using a distributor for even spread of particles. The illuminated particles simulate the suspended water droplets flowing through the curved duct. A laser sheet of 2 mm thick is generated by a green wave laser diode installed at the middle of the bend duct. A hatch made in the curved duct wall is used to install the camera normally to the laser sheet in order to catch the images of the flow structure downstream. An open-source tool (PIVlab) analyzed with MATLAB as suggested by Thielicke and Stamhuis [18] is used for the image processing program. The program processes enormous small sub-images of a particle between two successive points along the travelling path. In that manner, the displacement of particle during a prescribed time interval provides and draws the velocity vectors for the entire flow field.

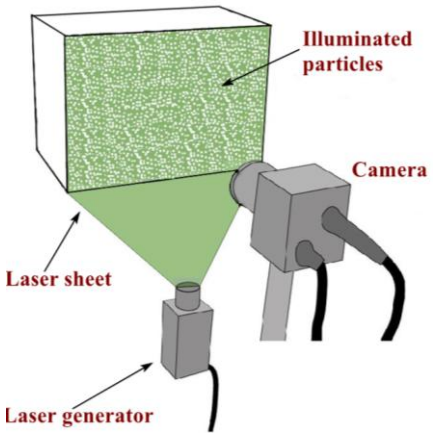

Figure 4. PIV system for flow visualization

C. Investigation Cases

The cases involved in both experimental and numerical investigations are conducted under the conditions listed in Table 1. The inlet boundary conditions those kept unchanged in all the tests are the inlet air temperature and relative humidity and water injection rate. In each case there will be implicitly three atomizer tilt angles ϕ to apply which are – 45º, 0º and 45º to the axial flow direction designated as a, b and c respectively. Thus for instance, case 1-b stands for test conducted at λ = 45º and ϕ = 0º with u_a = 2.5 m/s.

TABLE I. FLOW AND BOUNDARY CONDITIONS INVESTIGATED

Inlet air temperature			45ºC	
Inlet relative humidity			15%	
Water injection rate			19 kg/h	
Case	u_a (m/s)	λ	Re	Dn
1	2.5	45º	71500	63950
2	3.75	45º	107000	95700
3	5	45º	143000	127900
4	2.5	90º	71500	63950
5	3.75	90º	107000	95700
6	5	90º	143000	127900
7	2.5	135º	71500	63950
8	3.75	135º	107000	95700
9	5	135º	143000	127900

D. Physical Parameters

The most relevant physical quantities related to the evaporative cooling process are invested in the evaluation of experimental results. The air temperature and relative humidity are both reflect the eventual profit of spray cooling implemented in this study. Both air properties are normalised to the pretended ambient condition to make them more general and less relevant to the size and position of experimental facility used in current work. Hence, the non-dimensional average temperature and relative humidity of air at the end of test section are given in equations 1 and 2 below:

$$\theta = \frac{T}{T_{amb}} \tag{1}$$

$$\psi = \frac{RH}{RH_{amb}} \tag{2}$$

Where T and RH are the average air temperature and relative humidity for the 25 probes installed at the end of the duct. Average air temperature is determined by mass-weighted equation:

$$T = \frac{\sum \rho C_p u_i T_i A_i}{\sum \rho C_p u_i A_i} \tag{3}$$

Where ρ is density, C_p is constant pressure specific heat and u is velocity, all for humid air. A is area, and subscript i refers to a specified element in the duct cross section.

On the other hand, relative humidity is related to both temperature and water vapor content of the surrounding air. Therefore, it is determined as the ratio of actual RH in humid air to RH in saturated air at the same corresponding average air temperature:

$$RH = \frac{p_v(T)}{p_{vs}(T)} \tag{4}$$

Where p is the vapour pressure and notation vs denotes to the saturation state related to prevailed temperature.

In the same manner, the average air velocity measured by Pitot-static tube sliding along the duct cross section at entrance to the first straight duct is determined by area-weighted equation as:

$$u = \frac{\sum u_i A_i}{\sum A_i} \tag{5}$$

Finally the resultant cooling is best to be compared to the maximum available cooling motivated by the difference in temperature and water vapour content between the actual and saturation case. The physical quantity that realizes this comparison is the "Evaporative cooling effectiveness" defined as:

$$\varepsilon = \frac{T_{dbi} - T_{dbo}}{T_{dbi} - T_{wbi}} \tag{6}$$

© 2022 Int. J. Mech. Eng. Rob. Res

Where *dbi* and *dbo* are referred to dry bulb at inlet and exit of the test rig respectively. While *wbi* is the wet bulb at inlet condition.

III. Numerical Methodology

A. Geometric Model

The computational geometry for the spray cooling of air flow in a square duct comprises a curved section with a 0.75 curvature ratio as depicted in Fig. 2. The upstream section prior to the curved duct has a length of 3 m, while the length of the downstream section after the curve is 2 m. The heat and mass transfer region begins at the injection spot and ends downstream at the main test section before the fan entrance. This region may be changed in accordance to the position of the injection spot at 1.5, 1.0 and 0.5 m from the curved duct entry plane. However, in current simulation this distance is fixed at 1.5 m. Water is injected through nine atomizers, each with a 50° solid cone spray, and share the same water flow rate. The water atomizer can tilt in three directions 45°, 0° and – 45° relative to the axial air flow. All sides of the ducts are presumed to be adiabatic.

Three-dimensional, steady, incompressible, viscous flow has been adopted to study the flow structure through a curved duct at different bend angles. The ANSYS FLUENT 19.R1 commercial package is used in the numerical simulation relying on a discrete phase model (DPM) to solve for water droplets, while the continuous phase, i.e. air is treated as continuum.

The computational mesh used in the simulation is generated using ANSYS workbench. The hexagonal cell grid is chosen to fit the square geometry with refined cells close to the curved section to optimize the computations to the most accurate values. Five meshes are adopted to perform simulation with number of elements limited to the solution convergence. The grid independence test relies on the comparison of non-dimensional exit air temperature computed through mesh1, mesh2, mesh3, mesh4 and mesh5 having 1209420, 1897600, 2194246, 2542808 and 4264800 number of elements respectively. Fig. 5 demonstrates the final grid for numerical simulation with mesh3 as will be explained later in the results section. The simulation studies the effect of changing bend angle at three values 45°, 90° and 135° on the characteristics of the evaporative spray air cooling at steady state condition.

B. Governing Equations

The governing equations relevant to the case prescribed including the conservation equations and the turbulent model formulations. The mathematical formulation for the evaporation process encountered in the fogging system including two sections; Continuous phase flow and heat transfer representing air, and the dispersed phase flow and evaporation representing water droplets.

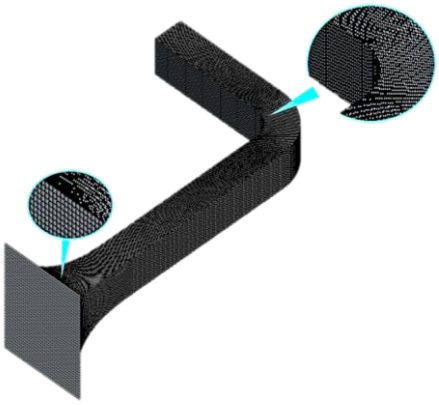

Figure 5. Computational grid for numerical simulation

1) Continuous Phase (Air)

The conservation equations for mass, momentum, energy and species are given below in vectorial notation through equations 7-10:

$$\nabla \cdot (\rho \vec{u}) = 0 \tag{7}$$

$$\nabla \cdot (\rho \vec{u}\vec{u}) = -\nabla p + \nabla \cdot \left[\mu\left(\nabla \vec{u} + \nabla \vec{u}^{T}\right)\right] + \rho \vec{g} \tag{8}$$

$$\nabla \cdot [\vec{u}(\rho e + p)] = \nabla \cdot \left(K_{eff} \nabla T - e_v \vec{j}_v\right) \tag{9}$$

$$\nabla \cdot (\rho \vec{u} Y_v) = -\nabla \cdot \vec{j}_v \tag{10}$$

Where μ is dynamic viscosity, g gravitational acceleration, e and e_v are enthalpies of humid air and vapour respectively. K_{eff} is effective thermal conductivity, j_v is vapour diffusion flux and Y_v is vapour mass fraction.

The RNG k-ε turbulent model adopted in the simulation presents equations 11 and 12 to calculate the turbulent kinetic energy k and the kinetic energy dissipation ε respectively:

$$\frac{\partial}{\partial x_i}(\rho k u_i) = \frac{\partial}{\partial x_i}\left(\alpha_k \mu_{eff} \frac{\partial k}{\partial x_i}\right) + G_k + G_b - \rho\varepsilon - Y_M + S_k \tag{11}$$

$$\frac{\partial}{\partial x_i}(\rho \varepsilon u_i) = \frac{\partial}{\partial x_i}\left(\alpha_\varepsilon \mu_{eff} \frac{\partial \varepsilon}{\partial x_i}\right) + C_{1\varepsilon}\frac{\varepsilon}{k}(G_k + C_{3\varepsilon} G_b) - C_{2\varepsilon}\rho\frac{\varepsilon^2}{k} + S_\varepsilon \tag{12}$$

Where G_k is the turbulent kinetic energy generated due to the mean velocity gradient, G_b is the turbulent kinetic energy generated due to buoyancy effects, Y_M is the added turbulent fluctuation to the overall dissipation rate. The inverse Prandtl numbers for k and ε are represented by α_k and α_e respectively. Also the terms S_k and S_e are stand for the user defined source terms, while C_{1e} , C_{2e} and C_{3e} are constants have values which are analytically calculated by Fluent.

2) Discrete Phase (Water Droplets)

The spray of water is immediately disintegrated into micro-size droplets after ejected out the atomizer. A thin film of air-water vapour forms outside the droplet surface motivating the mass and heat exchange between the air

© 2022 Int. J. Mech. Eng. Rob. Res

and the droplet. Mathematical formulation for water droplets considers the single-drop scheme evaporation to represent the mass and heat transfer.

In that manner, the energy equation for a droplet is described as:

$$m_d C_d \frac{dT}{dt} = hA_d\left(T_a - T_d\right) - \frac{dm_d}{dt} L_{fg} \tag{13}$$

Where m_d is droplet mass, C_d specific heat of droplet, t is time, h is convective heat transfer coefficient, T_a and T_d are air film and droplet temperature respectively. L_{fg} is latent heat of vaporization of water droplet.

The heat transfer coefficient is determined using the empirical correlation suggested by Faeth [19] corrected for $\mathrm{Re} \neq 0$:

$$Nu\frac{B_T}{1+B_T} = \frac{hd}{K} = 2 + \frac{0.555\,\mathrm{Re}^{0.5}\,\mathrm{Pr}^{0.33}}{\left[1+1.232/\left(\mathrm{Re}\,\mathrm{Pr}^{1.33}\right)\right]^{0.5}} \tag{14}$$

The Spalding thermal number B_T is determined by applying the Lewis analogy between mass and heat transfer solutions [20], thus:

$$B_T = B_m = \frac{Y_{vd} - Y_{va}}{1 - Y_{vd}} \tag{15}$$

The mass of water added to airstream, i.e. the evaporation rate of a droplet is given by:

$$\frac{dm_d}{dt} = K_m A_d\, \rho \ln\left(1 + B_m\right) \tag{16}$$

Where K_m is mass transfer coefficient, A_d droplet surface area and B_m is Spalding mass number.

The mass transfer coefficient is determined using the empirical correlation of Sherwood number [21]:

$$Sh = \frac{K_m d}{D_m} = 2 + \frac{0.555\,\mathrm{Re}^{0.5}\,Sc^{0.33}}{\left[1+1.232/\left(\mathrm{Re}\,Sc^{1.33}\right)\right]^{0.5}} \tag{17}$$

The non-dimensional parameters appear in equations 14 and 17 are given by the expressions:

$$\mathrm{Re} = \frac{ud}{\nu} \tag{18}$$

$$\mathrm{Pr} = \frac{\mu C_p}{K} \tag{19}$$

$$Sc = \frac{\mu}{\rho D_m} \tag{20}$$

Where ν is kinematic viscosity, D_m is mass diffusivity of vapour into air. Re, Pr and Sc are Reynolds number, Prandtl number and Schmidt number.

All properties involved in the parametric calculations above are representing the effective mean values determined on the bases of the mass fraction of water vapour or the humidity ratio of the air stream. Therefore, generally any property is determined by the mass weighted formula given by:

$$X = X_v Y_v + X_a\left(1 - Y_v\right) \tag{21}$$

Where X is to be replaced by μ, K, C_P..etc. The mass diffusivity of water vapour into air is determined by the expression [22]:

$$D_m = \frac{0.926\times10^{-6}}{p}\left(\frac{T^{2.5}}{T+245}\right) \tag{22}$$

The momentum equation represents the movement of a droplet in accordance to Newton's second law. The velocity of a droplet under the drag and gravity forces is given by:

$$\frac{du_d}{dt} = F_D\left(u_a - u_d\right) + \left(1 - \frac{\rho}{\rho_d}\right)g \tag{23}$$

Where F_D is drag force, u_a and u_d are air and droplet velocities, ρ_d is water density. The drag force is expressed as [23]:

$$F_D = C_D \frac{18\mu}{\rho_d d_d^2}\frac{\mathrm{Re}}{24} \tag{24}$$

The drag coefficient C_D of an evaporating droplet has a value of 0.44 according to the applied range of Re [24].

IV. Model Validation

A. Mesh Independency Test

The verification of the numerical simulation is needed to grant reliability to the acquired results. The numerical results are significantly influenced by the dimensions and quality of the proposed mesh. For that purpose, the air non-dimensional temperatures at the end of the duct are compared for six selective cases out of Table 1, by five different meshes as shown in Fig. 6. The meshes considered in verification are explained previously while describing the geometric model. As indicated in Fig. 6, the temperatures obtained by mesh1, mesh2 are clearly differing from mesh3. Also, the temperatures given by mesh4 and mesh5 are not much different but still show a discrepancy in a lower percentage. Nevertheless, comparing mesh3 and mesh4 gives very close trends such that the disparity is only about 0.18%. Therefore, to save time and cost of numerical simulation, mesh3 with 2194246 elements was chosen to perform numerical simulation.

B. Validation of Numerical Model

The current study simulation results are validated by comparing them with the experimental data acquired throughout the tests. Fig. 7 presents the comparison between the measured and simulated non-dimensional exit air temperature for cases (1 to 9) at the atomiser tilt angle of 0°. It is noticed from the figure that the simulated values are higher than those measured in all

© 2022 Int. J. Mech. Eng. Rob. Res

cases and the maximum deviation never exceeds 8% which is acceptable for practical consideration. The disparities are due partially to the measurements, as well as, to the presumption of complete droplets evaporation adopted in simulation.

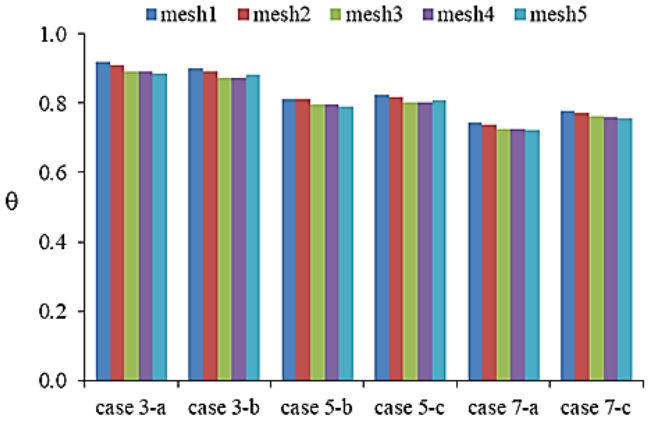

Figure 6. Mesh independence test

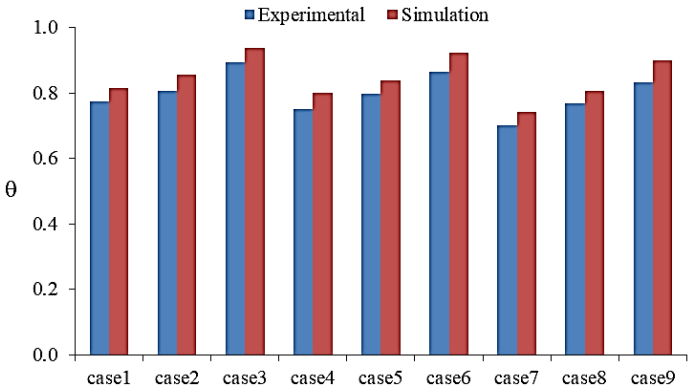

Figure 7. Comparison of non-dimensional exit ait temperature between experimental data and simulation results

Further validation of the results in current simulation is given in Fig. 8 by comparing the secondary vortices obtained currently with that of Boutabaa et al. [3] for bend angle 90º. The figure depicts the good agreement in topology of the flow in both studies by general trends and number of vortices. Still, the vortex core in current study goes little nearer to the inner wall due to the experienced higher Dean and Reynolds numbers.

V. Results and Discussion

This section is devoted to investigate the secondary flow structure within a curved duct with square cross section. The study focuses mainly on the effect of changing bend angle along with changing air velocity, and water atomizer tilt angle on the extent of evaporative cooling obtained by injecting water into the airflow.

The shape of the secondary flow vortices depends upon both the main flow conditions and the bend geometry. Figs. 9 and 10 illustrate the images captured experimentally by PIV for the secondary flow structure within the curved duct at different Dean numbers. The vortices developed with different bend angles at a velocity of 2.5 m/s are shown in Fig. 9. At bend angle 45º; it elucidates the development of a single pair of counter-rotating vortices closer to the outer wall of the duct due to the centrifugal forces push against the pressure gradient which induce an outward velocity component towards the outer wall. However, additional smaller pair of vortices appears with increasing Dean number while bend angle increases to 90º due to the intense mixing with the axial flow. Yet, further increasing the bend angle to 135º converts the flow scheme into four symmetric vortices as the growing rate of centrifugal effects has increased.

Increasing the air velocity leads to alter the relative positions of the secondary vortices as depicted in fig. 10. The figure shows for 90º bend that the pair of vortices nearer to the inner wall got closer as the velocity increased from 2.5 to 5 m/s. On the other hand, the pair nearer to the outer wall splits up along the duct midline and slightly moves away from the wall. This is attributed to the transport of the slow longitudinal region towards the outer wall along the symmetry plane.

From the foregoing it appears that the stronger interaction between centrifugal forces and the pressure gradient produced by increasing Dean number will certainly enhance the fluid mixing and rising the local relative velocities and rates of heat and mass exchange. The Dean vortices carry and rotate the suspended water droplets and aid the required penetration of them into the bulk air flow and the spiral motion keeps the strength of heat transfer downstream till the end of duct.

© 2022 Int. J. Mech. Eng. Rob. Res

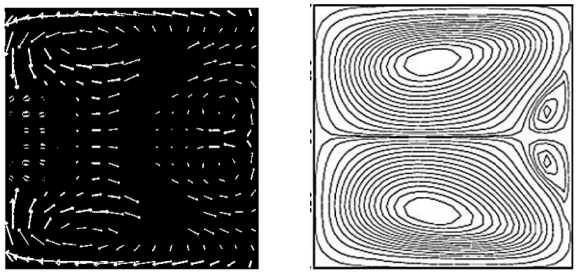

(a) (b)

Figure 8. Comparison for secondary flow structure obtained by simulation in current study with that of Boutabaa [3]

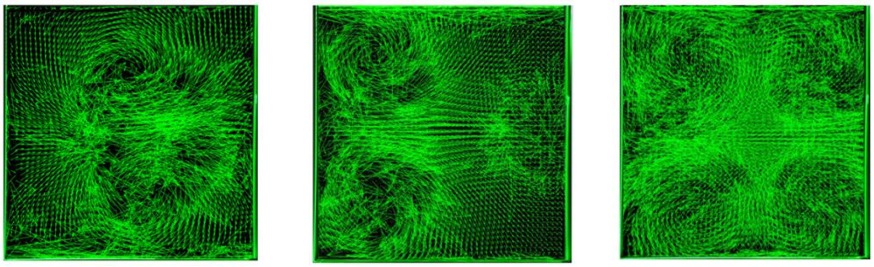

(a) (b) (c)

Figure 9. Flow structure at 2.5 m/s with different bend angles: a- 45º, b- 90º and c- 135º

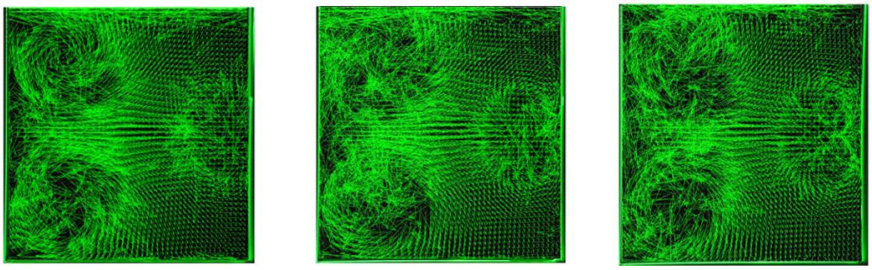

(a) (b) (c)

Figure 10. Flow structure of 90 °bend angle at different air velocity: a- 2.5 m/s, b- 3.75 m/s and c- 5 m/s

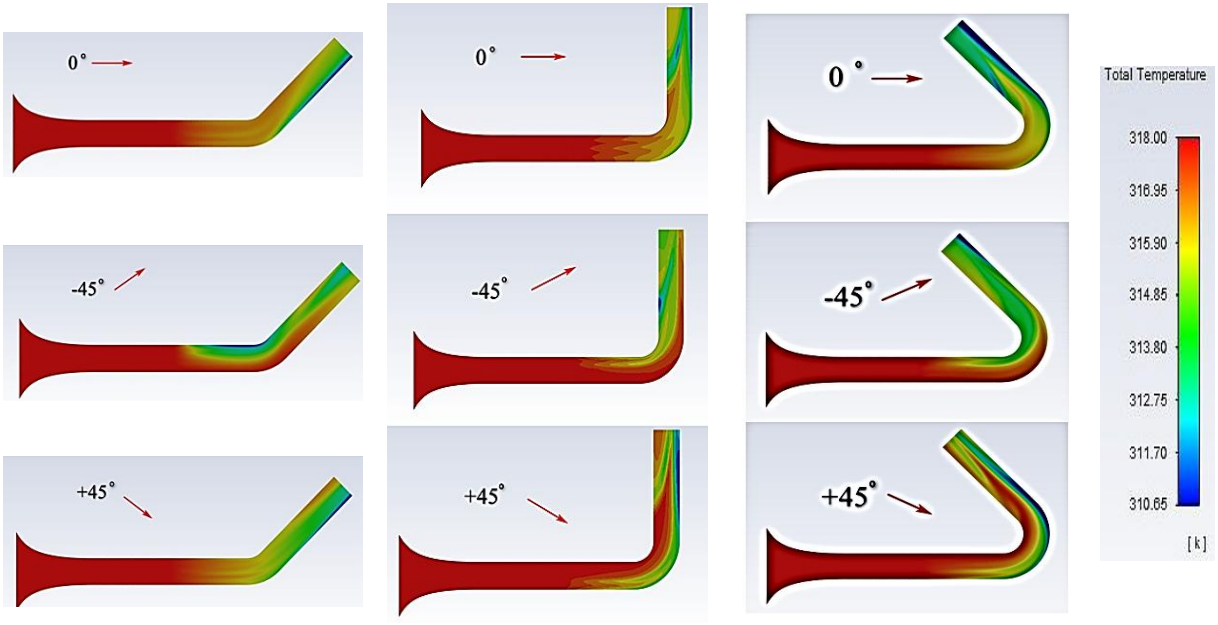

(a) (b) (c)

Figure 11. Temperature distribution of air in the (X-Z) planar for different bend angles for all atomizers tilt angles a- λ = 45º , b- λ = 90º and c- λ = 135º

© 2022 Int. J. Mech. Eng. Rob. Res

The local distribution of the injected water droplets carried by the air is essentially affected by the atomizer tilt angle across and downstream the curved duct. Fig. 11 shows the temperature-wise profiles of the air flowing along the square duct under varying flow conditions as predicted by numerical simulation. The air temperature is expected to remain constant until the air reaches the injection plane where micro-size water droplets are introduced into the flow. From that point onwards, a noticeable change in temperature appears that reflects the amount of evaporative cooling caused by humidifying the air influenced by the applied flow conditions. Generally, injecting the water towards the inner wall, i.e. at – 45º, makes the bulk of droplets trap within the inner vortices and travel along the separation zone closer to the inner wall. In this situation, the outer half air is almost remain dry and hot and meets the droplets at the end of duct where the mixing loses strength, thus leading to a relatively high average temperature there. On the other hand, if the water is injected towards the outer wall, i.e. at 45º, it seems better as most of the droplets spread across the duct and revolves with the vortices for 45º bend case. However, for the other bend angles, this tilt angle leads most of the droplets to be drifted outwards and gathered at the outer wall leaving the inner half of the duct to carry the warmer air beyond the separation zone where it meets the non-vaporised droplets. The delayed evaporation of the droplets is not adequate to achieve lower air temperature at duct exit and hence the average temperature is relatively high again. Among the three atomiser tilt angles which presents a superior droplets dispersion and higher cooling extent, is the one at which water is injected axially with the direction of air flow, i.e, at 0º. At this tilt angle the droplets are first uniformly spread prior to the curve and the cooling commences early there. Nevertheless, the droplets are then slightly drifted outwardly but keep a great portion revolving with the vortices while travelling through the curved duct. Such a case helps the droplets to penetrate the air flow and enhance the rates of evaporative cooling. The cooled air leaving the curved duct makes use of the spiral motion to mix with the rest of humidified stream and continue evaporation until the end of duct. For all bend angles the final average air temperature is the lowest in case of axially injected water, hence presenting the situation promising the best cooling characteristics for fogging technique of steadily flowing air stream like those encountered in the intake ducts of gas turbine power generators.

Fig. 12 demonstrates the average non-dimensional air temperature measured experimentally at the end of the test section which is representing the eventual cooling by fogging system under certain conditions. The figure reveals that tilting the injection with 45º gives the lowest cooling of the air in all cases at the three bend angles. Moreover, even if the injection is directed at -45º, better cooling with lower final temperature is attainable but still it is not the best case. The lowest final air temperatures are reached by axial injection, i.e. at 0º tilt angle, in all cases as depicted in Fig. 12. On the other hand, it is evident in the figure that decreasing the air velocity from 5 to 2.5 m/s will result in more cooling at all bend angles and injection tilting angles. Lower velocity offers longer time for the interaction between air and water droplets which increases the rate of evaporation. The cooling at the most favorable condition of 2.5 m/s and axial injection gives a temperature reduction of 22.8% at λ=45º, and a reduction of 24.4% and 30% for λ=90º and λ=135º respectively.

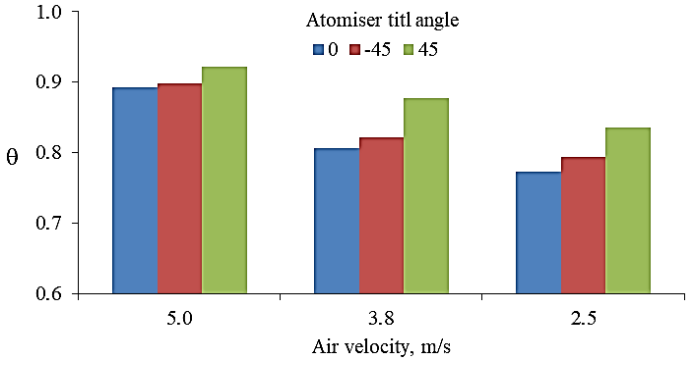

(a)

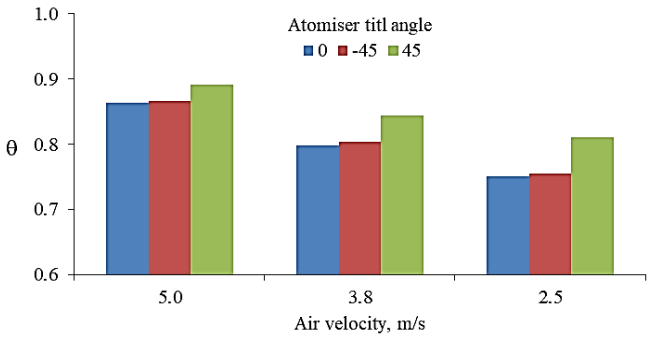

(b)

© 2022 Int. J. Mech. Eng. Rob. Res

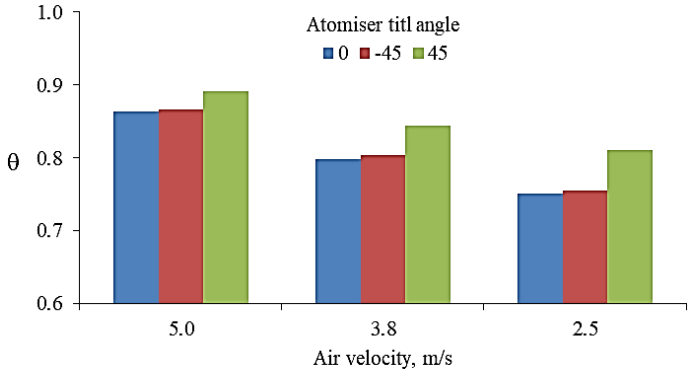

(c)

Figure 12. Non-dimensional exit air temperature obtained experimentally at different atomizers tilt angles a- $\lambda = 45^{o}$, b- $\lambda = 90^{o}$ and c- $\lambda = 135^{o}$

The lower temperature obtained by evaporative cooling are accompanied with increasing relative humidity of the treated air. Fig. 13 manifests the resultant relative humidity levels at various conditions measured experimentally. Under the same optimal conditions applied to non-dimensional temperature, i.e. at a velocity of 2.5 m/s and axial injection, the non-dimensional relative humidity increases by a factor of 2.67 at 45^{o} bend angle. However, the increase in relative humidity is 2.83 and 3.2 at bend angles 90^{o} and 135^{o} respectively. Generally, the characteristics of evaporative cooling have improved by 31.6% in air temperature and 19.9% in relative humidity when changing the bend angle from 45^{o} to 135^{o} at the most favorable conditions.

The resultant cooling can be fairly judged using the concept of cooling effectiveness, as elucidated in Fig. 14 at various attributed features of the work. The figure epitomizes the results of the work by showing the superiority of cooling effectiveness for bend angle 135^{o} over the other two bend angles. The effectiveness at bend angle 135^{o} excels that of 90^{o} by 16% and of 45^{o} by 26% under the optimal conditions.

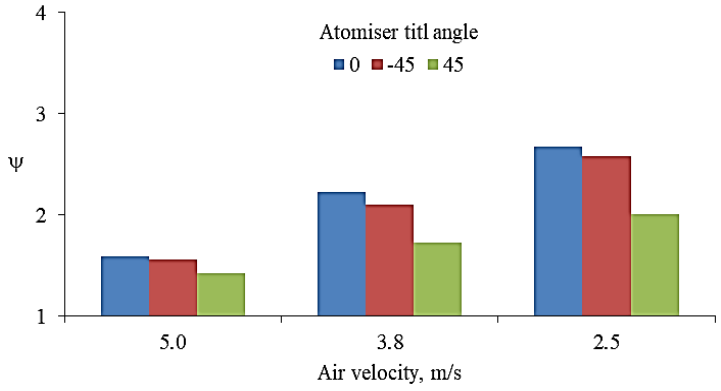

(a)

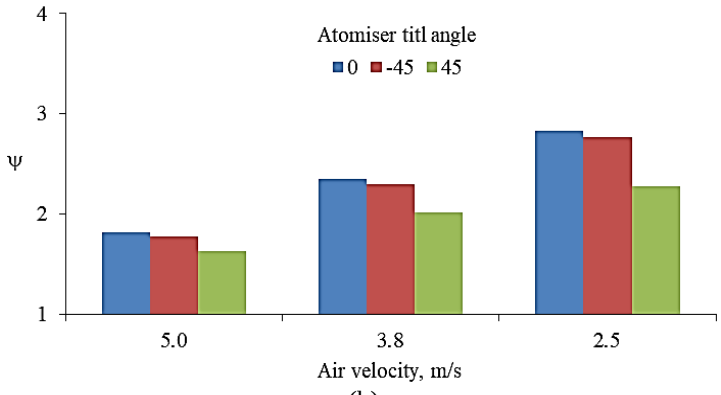

(b)

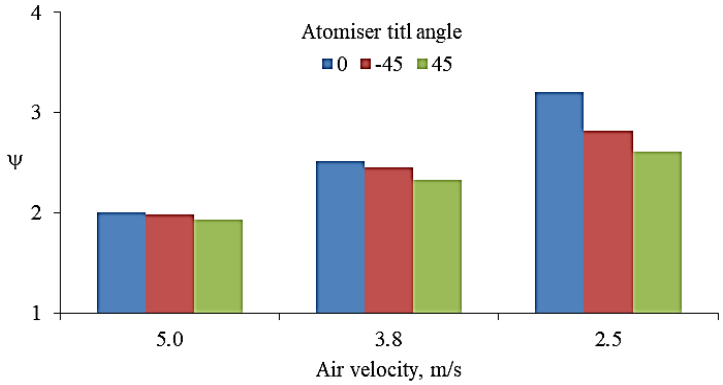

(c)

Figure 13. Non-dimensional exit air relative humidity obtained experimentally at different atomizers tilt angles a- λ = 45° , b- λ = 90° and c- λ = 135°

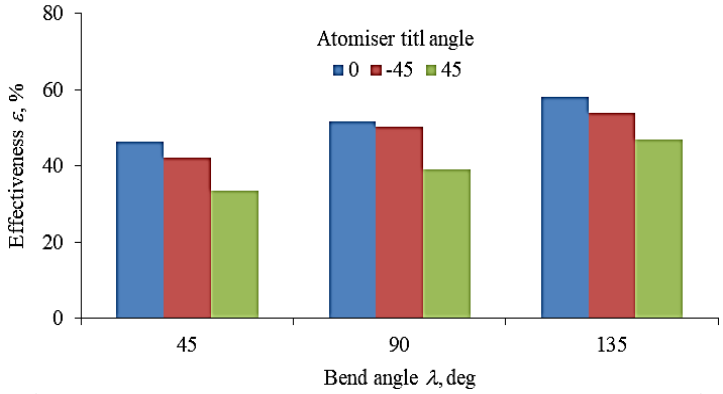

Figure 14. Effectiveness of evaporative cooling obtained experimentally at various atomizers tilt angles for different bend geometries

Nusselt number is the pronounced parameter to characterize the evaporative cooling of air flowing through the intended bend geometry. Fig. 15 demonstrates the functional relation between the humidified airflow represented by Re and the definitive heat exchanged between airstream and water droplets represented by Nu. The figure shows the anticipated trend of heat transfer improvement with increasing flow Re for all cases under inspection. At lower bend angle 45°, the relative locations of Nu lines are somewhat apart and the lowest is for tilt angle of 45°. The degradation in Nu with changing injection angle from 0° to 45° is about 11.3% , while change it to – 45° will degrade Nu by about 5% as an average. Nevertheless, for moderate bending at 90°, Nu is improved and the line for injection angle – 45° gets closer to that for 0° such that the deviation between the two lines is only 4% as an average. Yet, directing the injection in 45° yields an average deviation of 10.3% from that of 0°. More bending the curved duct to 135° brings better rate of increase in Nu particularly for 45° injection angle. The stronger and symmetrical vortices aid the flow agitating and improve phase mixing at this bend angle, thus enhance the heat exchange between air and water droplets. The increase in Nu with changing water injection from 45° to 0° is about 8.7%, while change injection to – 45° will bring only 5.6% average increase in Nu. Generally, examining the figure elucidates clearly that increasing bend angle will continuously improve Nu and brings more cooling to the air stream. For instance, at the favorable atomizer tilt angle, i.e. at 0°, the change in bend angle from 45° to 90° achieves an average improvement in Nu of 2.8%. However, changing the bend angle to 135° yields an improvement of 6.5% on average.

The foregoing indicates clearly the significant effect of bend angle on the flow structure and heat transfer for air exposed to evaporative cooling via water spray. Hence, according to the preceding discussion, the recommended bend geometry and flow characteristics for the intended fogging system are curved duct with 135 °bend angle and axial water injection, i.e. at 0 °. This realization must be considered when retrofitting a fogging system to gas turbine power generators and redesign of the inlet ducts incorporating curved section becomes decisive.

VI. Conclusion

The most important outcomes of this study concerning the bend angle influence upon the evaporative cooling of airstream flowing throughout the curved square ducts can be summarized as:

- Lower air velocity gives better cooling characteristics due to the longer time available for the mass and heat exchange between the injected water and the airstream.
- Increasing the bend angle from 45° to 90° generates one more pair of vortices, yet, at the bend angle of 135°, the four vortices are similar in size and

strength due to the higher Dean and Reynolds numbers.

- Injecting the water towards either the inner or the outer duct walls leaves the opposite half of the curved duct almost dry and hot. This effect will give a higher average air temperature at the end of duct. This observation was common for the all bend angles.
- The best characteristics for the evaporative cooling are obtained when the water has sprayed axially along the flow direction, i.e. at 0° tilt angle. This is considered the optimum atomizers position.
- Nu is enhanced with increasing bend angle, as well as, increasing Reynolds number. Changing bend angle from 45° to 135° will bring an enhancement of 6.5% in Nu number.
- The recommended preferable operating condition of the fogging system is defined by 0° atomizer tilt angle through 135° bent duct. The utmost cooling effectiveness obtained in this condition exceeds the 45° bend by 26% and the 90° bend by 16%.

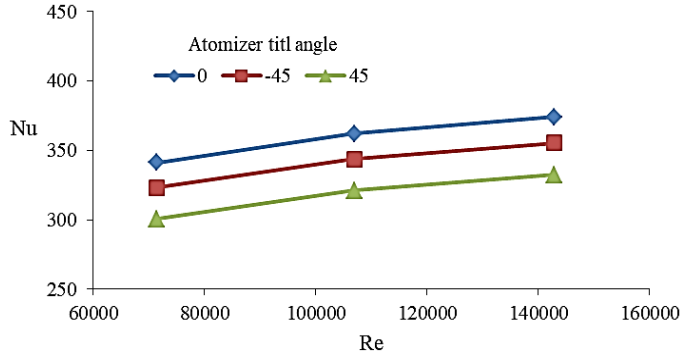

(a)

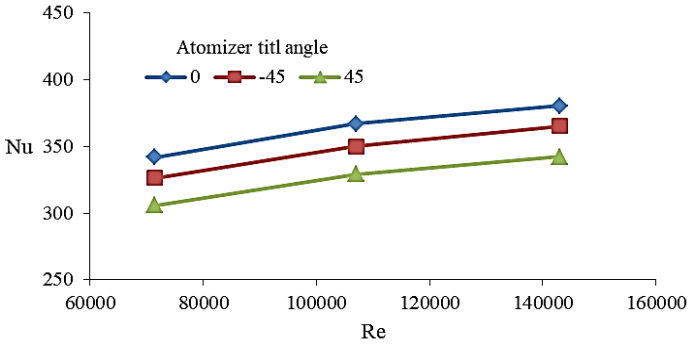

(b)

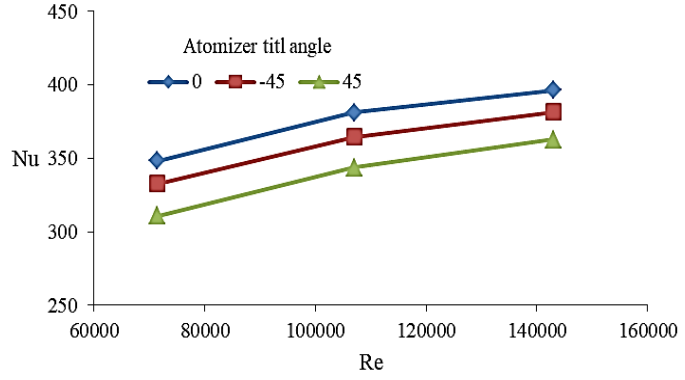

(c)

Figure 15. Nusselt number VS Reynolds number for evaporating droplet at various atomizers tilt angles
a- λ = 45° , b- λ = 90° and c- λ = 135°

CONFLICT OF INTEREST

The authors declare that they have no known competing financial interests or personal relationships that could have appeared to influence the work reported in this paper.

AUTHOR CONTRIBUTIONS

Akeel A. Nazzal: Conducting research and writing original draft/review editing.

Abdulsattar J. Hasan: Supervision, conceptualization and validation. Both authors had approved the final version.

© 2022 Int. J. Mech. Eng. Rob. Res

REFERENCES

[1] W. Dean, "Fluid motion in a curved channel," in *Proc. the Royal Society of London*. Series A, 121, 787, 1928.

[2] K. Sudo, M. Sumida, H. Hibara, "Experimental investigation on turbulent flow in a circular-sectioned 90-degree bend," *Experiments in Fluids*, vol. 25, 1998.

[3] M. Boutabaa, L. Helin, G. Mompean, and L. Thais, "Numerical study of dean vortices in developing Newtonian and viscoelastic flows through a curved duct of square cross-section," *C. R. Mecanique*, 337, 2009.

[4] D. Al-Khafaji and Abdur Rahim, "The computation of swirling flows," *International Journal of Mechanical Engineering and Robotics Research*, vol. 1, no. 1, 2012.

[5] D. Arvanitis, D. Bouris, and E. Papanicolaou, "Laminar flow and heat transfer in U-bends: The effect of secondary flows in ducts with partial and full curvature," *International Journal of Thermal Sciences*, vol. 130, 2018.

[6] S. Mondol, M. I. Hossain, M. Tajul Islam, "Characteristics of gas flow through bend pipes of different angles," *IOSR Journal of Mathematics*, vol. 14, no. 6, 2018.

[7] S. Shabani, A. Abedini, and A. Mohammadtabar, "The effect of the pipe bending angle on the pressure losses vane elbow pipes," *Asian Review of Civil Engineering*, vol. 8, no. 1, 2019.

[8] R. Mondal, M. Zohurul Islam, M. Minarul Islam, and S. Yanase, "Numerical study of unsteady heat and fluid flow through a curved rectangular duct of small aspect ratio," *Thammasat International Journal of Science and Technology*, vol. 20, no. 4, 2015.

[9] M. Z. Islam, R. Mondal, and M. Rashidi, "Dean-Taylor flow with convective heat transfer through a coiled duct," *Computers & Fluids*, vol. 149, 2017.

[10] M. Zohurul Islam, R. Mondal, and S. Saha, "Impacts of rotation on unsteady fluid flow and energy distribution through a bending duct with rectangular cross section," *Energy Engineering*, vol. 119, no. 2, 2022.

[11] M. Hasan, R. Mondal, M. Zohurul Islamc, and G. Lorenzinid, "Physics of coriolis-energy force in bifurcation and flow transition through a tightly twisted square tube," *Chinese Journal of Physics*, vol. 77, 2022.

[12] J. Azzola, J. Humphrey, H. Iacovides, and B. Launder, "Developing turbulent flow in a u-bend of circular cross-section: measurement and computation," *ASME Trans*., vol. 108, 1986.

[13] G. Lee, Y. Choi, and S. Han, "Measurement of developing turbulent flow in a u-bend of circular cross section," *Journal of Mechanical Science and Technology*, vol. 21, no. 2, 2007.

[14] A. Jain, "Experimental investigation of turbulent flow in a pipe bend using particle image velocimetry," M.Sc. thesis, McMaster Univ., Canada, 2017.

[15] S. Bhattacharya, J. Charonko, and P. Vlachos, "Particle image velocimetry (PIV) uncertainty quantification using moment of correlation (MC) plane," *Meas. Sci. Technol.* vol. 29, no. 11, 2018.

[16] S. Eiamsa-ard, K. Kunnarak, K. Wongcharee, and V. Chuwattanakul, "Heat transfer visualization of swirling impinging jets using nozzle with centrally hollow helical-tape," *International Journal of Mechanical Engineering and Robotics Research*, vol. 9, no. 5, 2020.

[17] A. Mohammed and S. Abed-Alfathel, "The effect of curvature ratio on flow structure and fluids mixing in 90° bent square duct," *Journal of University of Babylon for Engineering Sciences*, vol. 28, no. 2, 2020.

[18] W. Theielicke and E. Stamhuis, "PIVlab-Towards user-friendly, affordable and accurate digital particle image velocimetry in MATLAB," *Journal of Open Resource Software*, vol. 2, 2014.

[19] G. Faeth, "Current status of droplets and liquid combustion," *Progress in Energy and Combustion Sciences*, vol. 3, 1977.

[20] S. Sazhin, "Advanced models of fuel droplet heating and evaporation," *Progress in Energy and Combustion Sciences*, vol 32, 2006.

[21] S. Sazhin, I. Shishkova, A. Kryukov, V. Levashov, and M. Heikal, "Evaporation of droplets into a background gas: Kinetic modeling," *International Journal Heat Mass Transfer*, vol. 50, 2007.

[22] Mass Transfer, ASHRAE Fundamentals Handbook, SI version, 1997.

[23] W. Chen, D. Chong, J. Yan, S. Dong, and J. Liu, "Numerical investigation of two-phase flow in natural gas ejector," *Heat Transfer Engineering*, vol. 35, 2014.

[24] G. Faeth, "Evaporation and combustion of sprays," *Progress in Energy and Combustion Sciences*, vol. 9, 1983.

Copyright © 2022 by the authors. This is an open access article distributed under the Creative Commons Attribution License (CC BY-NC-ND 4.0), which permits use, distribution and reproduction in any medium, provided that the article is properly cited, the use is non-commercial and no modifications or adaptations are made.

Akeel A. Nazzal received his B.Sc. degree in Air-conditioning from University of Technology, Iraq in 2014, and M.Sc. degree in Air-conditioning from University of Technology, Iraq in 2021. He worked as design and sales engineer of central air conditioning systems in Hexacorp of Carrier. Currently he is working for Martyrs Foundation.

Abdulsattar J.M.Hasan received his B.SC. degree in Air-conditioning engineering from University of Technology, Iraq in 1989, M.Sc. in Power generation from University of Technology-Iraq in 1994, and Ph.D. in Thermal sciences from University of Technology-Iraq in 2010. He served as a consultant for many industrial facilities in Iraq till 2003. He worked as a Training Manager for SKM Air-Conditioning Equipment, UAE in 2007. Currently, he is an Assistant Professor in Mechanical Engineering Department, University of Technology, Iraq. His current research interests are in fields of Internal Combustion Engines, Combustion, Bio-Fuels Technology, Multi-Phase flow, Heat and Mass transfer, and Air-conditioning.